NMPC-based Integrated Thermal Management of Battery and Cabin for Electric Vehicles in Cold Weather Conditions

Mohammad R. Hajidavalloo, Jun Chen*, Senior Member, IEEE, Qiuhao Hu, Ziyou Song, Member, IEEE, Xunyuan Yin and Zhaojian Li, Senior Member, IEEE

Abstract—One of the major obstacles along the way of electric vehicles' (EVs') wider global adoption is their limited driving range. Extreme cold or hot environments can further impact the EV's range as a significant amount of energy is needed for cabin and battery temperature regulation while the battery's power and energy capacity are also impeded. To overcome this issue, we present an optimal control strategy based on nonlinear model predictive control (NMPC) for integrated thermal management (ITM) of the battery and cabin of EVs, where the proposed NMPC simultaneously optimizes the EV range and cabin comfort in real time. Firstly, the components of the designed ITM system are introduced and control-oriented modeling is done. Secondly, to demonstrate and validate the benefits of the proposed ITM, an optimal control problem is defined and dynamic programming (DP) is employed to find the global optimal solution. Thirdly, for practical implementation, NMPC-based control strategy is developed, where the cost function design and weights calibration are done in comparison with DP global optimal solution. Weight-tuning results show that our NMPC-based approach can achieve close driving range maximization as compared to the DP benchmark while ensuring cabin comfort. The developed NMPC-based ITM strategy is further illustrated by comparing its performance to two additional benchmark strategies, i.e., rulebased control and cabin heating only. Finally, our simulation results also identify several important factors that impact the benefits of the proposed NMPC-based ITM, which are used to summarize the operating conditions under which the proposed ITM is critically needed.

Index Terms—Model predictive control, electric vehicles, thermal management, cabin comfort.

I. INTRODUCTION

Electric vehicles (EVs) will comprise a significant portion of the transportation fleet in the foreseeable future, due to the

Manuscript received December 29, 2022; revised February 26, 2023, April 6, 2023, and May 1, 2023; accepted May 8, 2023. (Corresponding author: Jun Chen.)

Mohammad Hajidavalloo and Zhaojian Li are with the Department of Mechanical Engineering, Michigan State University, East Lansing, MI 48824, USA. Email: {hajidava, lizhaojl}@msu.edu.

Jun Chen is with the Department of Electrical and Computer Engineering, Oakland University, Rochester, MI 48309, USA. Email: junchen@oakland.edu.

Qiuhao Hu is with the Department of Naval Architecture & Marine Engineering, University of Michigan, Ann Arbor, MI 48109, USA. Email: qhhu@umich.edu.

Ziyou Song is with the Department of Mechanical Engineering, National University of Singapore, Singapore 117575. Email: ziyou@nus.edu.sq.

Xunyuan Yin is with the School of Chemistry, Chemical Engineering and Biotechnology, Nanyang Technological University, 62 Nanyang Dr, 637459, Singapore. Email: xunyuan.yin@ntu.edu.sg.

financial effect of fluctuating oil prices, the growing public interest in green and renewable technologies, and regulations and policies for upcoming fuel economy standards [1]–[8]. For example, California will ban sales of new gasoline-powered cars by 2035 [9]. However, there are still several obstacles for widespread adoption of EVs, including the higher marginal price of EVs relative to conventional vehicles, limited driving range, degenerated performance in low temperatures, and safety and stability concerns in high temperatures and autonomous driving mode, to name a few [1], [10]–[15].

In particular, cold weather conditions have three major effects on EVs. Firstly, cold weather itself leads to degraded Liion battery performance in terms of lower available energy and power capacity as well as reduction in battery life. Generally, the poor performance of Li-ion batteries in cold weather results from the significant increase of battery internal resistance, which leads to a strong opposing force on a running battery [16]. Furthermore, the Li-ion battery cell anode may experience lithium plating, a dangerous mechanism in low temperatures, which causes a reduction in the energy and power capabilities of the Li-ion battery and severe battery degradation [17]. Secondly, the driving range of EVs is also adversely affected by cold weather due to the restricted regenerative charging, limited propulsion power, and reduced capacity, etc. To this end, 13% all-electric-range reduction for a plug-inhybrid EV operating at -7 °C ambient temperature, compared to driving at 0 °C, is reported for a battery hardware-in-theloop study conducted at Argonne National Laboratory [18]. Note that nearly 34% and 12% of this range reduction is due to the restricted regenerative power and increased thermal resistance, respectively [18]. Thirdly, to mitigate the negative impact of cold weather, a significant portion of battery energy is used for the purpose of controlling the cabin and battery temperatures, resulting in EV range reduction. In addition to the EV performance degradation, the control design for EV thermal management becomes more challenging with the inclusion of cabin temperature regulation and more harsh environmental circumstances.

Due to the challenges brought on by cold weather conditions as outlined above, thermal management strategies for EVs have started to penetrate the market, and extensive research efforts have been taken on this subject. From a control engineering standpoint, the literature has addressed the thermal management of the battery and/or cabin for heating or cooling using methods such as nonlinear model predictive control

1

(NMPC) [19]–[26], fuzzy-logic control [27], dynamic programming (DP) [28]–[30], and PID control [31], [32], with the majority of the works being concerned with cooling controls. For example, [28] proposes an iterative DP-based battery thermal management strategy for connected and automated hybrid EVs. References [19], [23], [33] are based on (N)MPC, where their objective is to minimize the energy consumption of the thermal management system while satisfying various constraints. In [21], [22], vehicle connectivity is assumed and multi-layer MPC is developed to improve the battery energy efficiency.

In the context of battery and cabin heating, there are a few prior works [18], [20], [34], [35]. Authors in [20] studied the battery thermal management of intelligent connected EVs at low temperatures based on NMPC, where heat pump (HP) with an electric heater is used to provide heat for the liquid heating loop for battery temperature regulation. The results demonstrate that the developed strategy can reduce the heating time and energy consumption. NMPC is also used for control of cabin temperature and air quality in EVs equipped with HP in cold weathers [34]. Rule-based control of battery external heating for EVs during driving at low temperatures is also studied in [35], where in this case the driving range of an EV is compared with the case where maximum heating power is used as well as with the case when battery is not heated. Promising improvements are reported in [35].

Despite these progresses, the integrated cabin and battery thermal management for extreme cold condition has not been thoroughly investigated in the literature. Specifically, the interaction between the driving range, cabin comfort, and power consumption of the thermal management (TM) system has not been fully evaluated, particularly at subzero temperatures. Note that in the existing works that have similar scope [18], [35]–[37], the models and the made assumptions in these works may not accurately reflect the battery performance in low temperatures, and certain important cabin/battery aspects are neglected. For example, in [35], the regenerative power loss is overlooked in the quantification of the range loss, which in fact is one of the major energy loss sources in below-freezing conditions [18], [36].

In this paper, we present an NMPC-based integrated thermal management (ITM) of battery and cabin in cold weather conditions, with the focus on its effect on the driving range of EVs and cabin comfort requirements. Our findings show that there exist important trade-offs among battery performance improvement (due to the battery temperature rise), the cabin comfort requirements, and the power consumption of the thermal management system. Furthermore, our simulation results demonstrate that the advantages of an increase in EV range resulted from battery heating depend on many factors and circumstances, such as ambient temperature, driving cycle profile and behavior, control strategies, driving time, etc. The NMPC's capability to effectively forecast the future system trajectories for a sufficiently long time is another important aspect related to the control design phase.

Our contributions and key advancements are summarized as follows.

1) A unified, integrated and comprehensive thermal man-

- agement problem is formulated, by developing controloriented models for each component and comprehensively considering conflicting metrics and constraints.
- 2) An efficient NMPC-based ITM strategy is developed to simultaneously optimize EV driving range and cabin comfort while dealing with system constraints. Dynamic programming is employed to provide the optimal global reference to fine tune the cost functional terms in NMPC for achieving improved performance.
- 3) Simulations of the proposed NMPC-based ITM strategy, together with two benchmark control strategies, including rule-based control and cabin heating only, are carried out to demonstrate the effectiveness of the proposed approach and to identify factors and conditions under which the proposed ITM is critically needed.

To the best of the authors' knowledge, this is the first study that provides modeling of integrated thermal management of battery and cabin for control purposes with a focus on comprehensive investigation on the EV driving range and cabin comfort in cold weather conditions.

The rest of the paper is structured as follows. In Section II, the proposed ITM system for battery and cabin heating are introduced with models for major components. The NMPC problem, together with the investigation of its stage cost design and calibration, is discussed in Section III, whereas in Section IV, simulation results are presented with discussions. Finally, Section V concludes the paper.

II. DESIGN & MODELING

We begin this section with an overview of the operation conditions of the proposed ITM design for battery and cabin. Specifically, the coolant cycle of the ITM system (for heating) under examination is depicted in Fig. 1. First, the coolant with a flow rate of \dot{m} and a temperature of T_4 is heated by the HP to T_1 . The heated coolant is then directed to the 3way valve, where the controller governs the coolant flow rates for the cabin and battery branches. The coolant flow for the cabin heating, whose flow rate is denoted by \dot{m}_c , passes the heat exchanger (HX) and indirectly heats the inlet air to the cabin and becomes cooled. The inlet air to the cabin heats the cabin air and then transfers back to the HX to complete the cycle. On the battery side, the coolant flowing through the battery branch heats the battery, whose flow rate is denoted by \dot{m}_b . The coolant cycle is then completed when the coolant flow for the cabin and battery is mixed to achieve temperature T_4 . We go into further detail about each part of the proposed integrated battery and cabin thermal management system in the subsections that follow. The list of notations for the proposed ITM systems is provided in Table I.

A. Heat pump model

As shown in Fig. 1, the coolant with low temperature T_4 is heated by an HP, the heat rate of which is denoted by \dot{Q}_{HP} . The coolant then reaches a higher temperature T_1 that is necessary for further circulation of the coolant to heat the

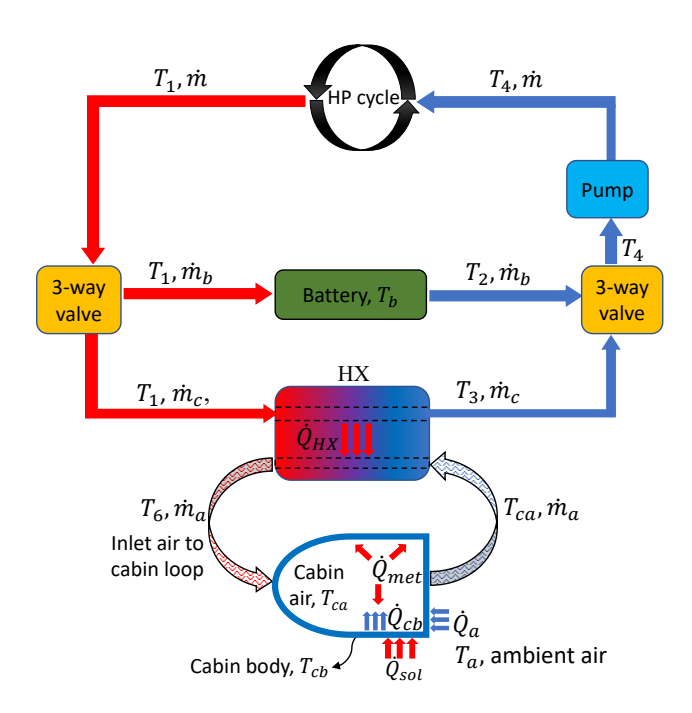


Fig. 1: Schematics of the integrated battery and cabin thermal management (heating) system.

TABLE I: Notations for the Proposed ITM

Notation	Physical meaning			
T_1	coolant temp. after HP			
T_2	clnt. temp. after heat exch. with battery			
T_3	clnt. temp. after heat exch. with cabin	^{o}C		
T_4	coolant temp. after mixing			
T_b	battery temp.			
T_6	inlet air to cabin temp.			
T_{ca}	cabin temp.			
T_{cb}	cabin body temp.	^{o}C		
\dot{m}_c	cabin branch coolant flow rate	$\frac{kg}{s}$		
\dot{m}_b	battery branch coolant flow rate	$\frac{kg}{s}$		
\dot{m}	total coolant flow rate	$\frac{kg}{s}$		
n_{comp}	compressor speed	rpm		

cabin and the battery as will be shown in the subsequent texts. The governing equations for this heat exchange are:

$$C_1 \dot{T}_1 = \dot{Q}_{HP} + \dot{m}c_c(T_4 - T_1),$$
 (1a)

$$\dot{m} = \dot{m}_b + \dot{m}_c,\tag{1b}$$

where $C_1 = m_{clnt}c_c$ is the thermal inertia of the heated coolant, m_{clnt} is the total mass of the coolant in the cycle, c_c is the specific heat capacity of the coolant, and \dot{m} is the total coolant flow rate. The coolant liquid is G-48 ethyleneglycol which is a common choice for vehicles thermal loop. The main advantage of employing HP instead of PTC (positive temperature coefficient) heaters is that it has a coefficient of performance (COP) greater than one, thus improving the range

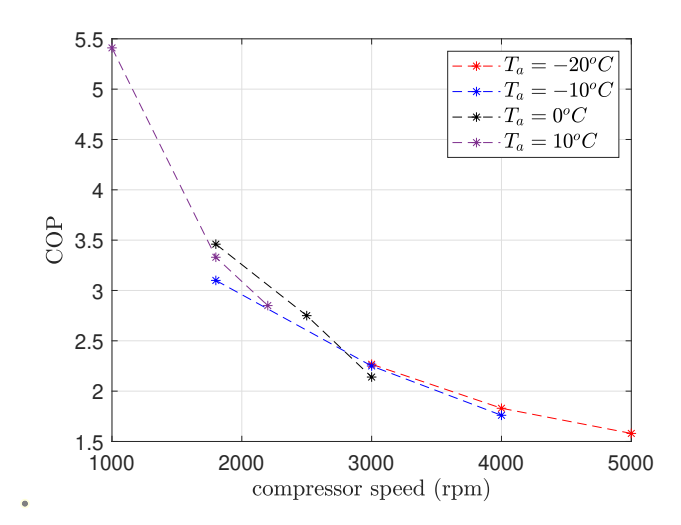


Fig. 2: COP of the proposed ITM at different ambient temperatures based on to experimental data of reference [40]

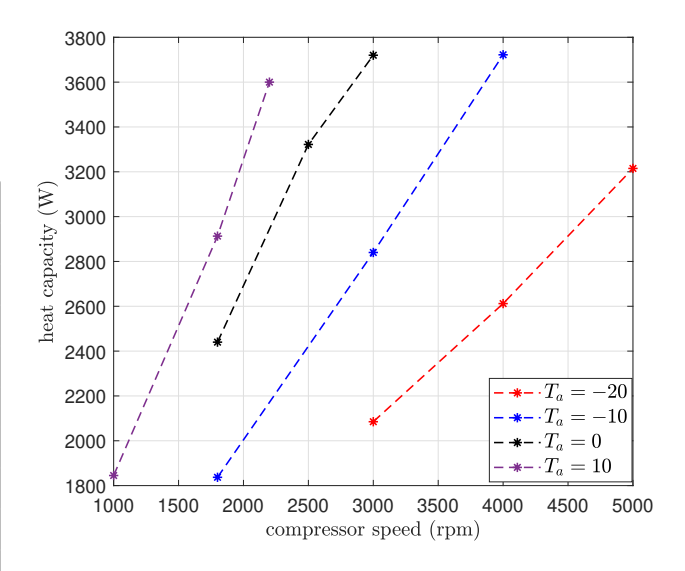


Fig. 3: Heat capacity of the proposed ITM at different ambient temperatures based on to experimental data of reference [40]

of EVs. Note that HP has already been deployed by EV makers such as Tesla (e.g., Tesla Model Y) and Nissan (e.g., Nissan Leaf) [38], [39].

In this paper, we consider ambient temperatures and compressor speeds as variables and assume fixed indoor air recirculated percentage and outdoor air velocity. Thus, the heat provided by HP follows from the definition of the COP, i.e.,

$$COP_{HP}(T_{amb}, n_{comp}) = \frac{\dot{Q}_{HP}(T_{amb}, n_{comp})}{P_{elec}}, \quad (2)$$

where \dot{Q}_{HP} is the heat capacity, P_{elec} is the electric power consumption of the HP mostly from compressor, and COP_{HP} stands for the coefficient of performance of the HP cycle. In this regard, we take the compressor speed, n_{comp} , into consideration as another control variable. After n_{comp} is decided upon and T_a is known, the experimental data studied

in [40] can be utilized to calculate the HP's electrical power consumption. In [40] the performance of an EV's HP is evaluated experimentally in cold climate conditions where the results are summarized in Figs. 2 and 3. In these two figures, COP and heat capacity of the EV's HP are shown at various ambient temperature and compressor speeds. According to the findings of [40], at a fixed ambient temperature, fixed indoor air recirculated percentage, fixed outdoor air velocity and fixed inlet air flow rate, COP and heat capacity change linearly w.r.t compressor speed so one can easily interpolate the performance of the HP based on the experimental data. Interested readers are referred to [40] for more details on the experiments resulting in quantifying the HP performance.

B. Cabin heat exchanger (HX) and cabin dynamics

It is generally difficult to model the thermal dynamics of a vehicle cabin, especially if it includes an HVAC system, as there are many factors and variables to take into consideration [34]. The model should be sufficiently detailed to correctly forecast the cabin's thermal behaviors. In the meantime, a low-complexity, control-oriented model is favored due to realtime computation constraints. In this regard, we follow the developments in [34], [41] for modeling the inlet air to cabin heat exchange as well as the cabin air dynamics. As previously mentioned, the coolant flow rate for the cabin branch, \dot{m}_c , passes through an HX with high temperature T_1 to heat the inlet air to cabin and exits the HX with low temperature T_3 . The heated inlet air with high temperature T_6 enters the cabin with flow rate \dot{m}_a , heats the cabin air with temperature T_{ca} , reaches the cabin temperature, and then exits the cabin. As a result, the following two equations can be used to model the heat exchange between the coolant and the cabin inlet air loop:

$$C_3 \dot{T}_3 = \dot{m}_c c_c (T_1 - T_3) - G_{HX} (T_3 - T_6),$$
 (3a)

$$C_6 \dot{T}_6 = c_a \dot{m}_a (T_{ca} - T_6) + G_{HX} (T_3 - T_6),$$
 (3b)

where (3a) models the heat exchange for the coolant flow in the cabin branch HX and (3b) characterizes the heat exchange for the inlet air to cabin mass. In these two equations, $C_3 = m_{clnt,c}c_c$ is the thermal inertia of the coolant in the cabin branch, $m_{clnt,c}$ stands for the cabin branch coolant mass, $C_6 = m_a c_a$ is the thermal inertia of the inlet air to cabin, m_a is the inlet air mass, c_a is the specific heat capacity of air, and G_{HX} is the heat transfer coefficient between the inlet air and the coolant.

For modeling the various elements of cabin components, it should be noted that the cabin air – the most important element for the thermal management task – has interaction with the inlet air to the cabin, the cabin body, cabin shell and interior, the passengers, and solar radiation, etc. The inlet air to the cabin serves as the primary heating element of the cabin components. For modeling the cabin dynamics, we consider the following second order model [41], [42] with the cabin air

temperature and cabin body temperature as state variables:

$$C_{ca}\dot{T}_{ca} = \dot{m}_{a}c_{a}(T_{6} - T_{ca}) + \dot{Q}_{met} + \alpha_{cb}A_{cb}(T_{cb} - T_{ca}), \tag{4a}$$

$$C_{c}\dot{T}_{ca} = -\alpha_{c}A_{c}(T_{c} - T_{c}) + \dot{Q}_{cc}A_{cb}(T_{cb} - T_{ca}), \tag{4a}$$

$$C_{cb}\dot{T}_{cb} = -\alpha_{cb}A_{cb}(T_{cb} - T_{ca}) + \dot{Q}_{sol} + \alpha_{ab}A_{ab}(T_a - T_{cb}),$$
(4b)

where (4a) represents the cabin air temperature dynamics, and (4b) represents the vehicle body temperature dynamics. Equation 4a summarizes the most important factors that affect the cabin air temperature, including the inlet air to cabin (the first term on the right), \dot{Q}_{met} that accounts for the metabolic heat from the passengers, and the heat exchange with other components such as cabin shell, window, and wall (as represented by the last term and denoted by heat exchange with cabin body). In Equation 4a, α_{cb} is the lumped heat transfer coefficient per unit area, A_{cb} is the heat transfer surface area between the cabin air and cabin body, T_{cb} is the cabin body temperature, and lastly $C_{ca} = m_{ca}c_a$ is the cabin air thermal inertia with m_{ca} being the cabin air mass. In Equation 4b, the first term on the right side accounts for the heat transfer from cabin air to the cabin body; the second term accounts for the heat absorbed by the sun; and the last term accounts for the heat transfer between the ambient air and the cabin body. Here $C_{cb} = m_{cb}c_{cb}$ is the cabin body thermal inertia with m_{cb} being the cabin body mass and c_{cb} being the specific heat capacity of the cabin body.

C. Pump model

According to Fig. 1, the pump is positioned after the 3-way valve that mixes the coolant flow from the battery and cabin before it reaches HP. The fluid's mixing temperatures can be determined as

$$T_4 = \frac{1}{\dot{m}}(\dot{m}_b T_2 + \dot{m}_c T_3). \tag{5}$$

The pump is tasked to maintain the desired flow rate by performing mechanical work to the coolant. The power consumption of the pump is represented by:

$$P_{pump} = \frac{P_{pump,m}}{\eta_m} = \frac{1}{\eta_m} \cdot \frac{\Delta p_{pump} \dot{m}}{\rho_c}, \tag{6}$$

where $P_{pump,m}$ is the mechanical power, η_m is the power conversion rate of the pump, ρ_c is the coolant density, Δp_{pump} is the pressure drop of the pump, which is related to the mass flow rate of the coolant according to follows [20]:

$$\Delta p_{pump} = 0.927\dot{m}^2 + 0.586\dot{m} - 0.143. \tag{7}$$

D. Electrothermal battery model and battery pack

The battery cell used to construct the battery pack is modeled using the popular Equivalent Circuit Model (ECM) [8], [16], [43]–[45]. As shown in Fig. 4, V_{oc} denotes the open-circuit voltage of the cell; R_o is the ohmic resistance; R_p and C_p are the polarization resistance and capacitance respectively. Furthermore, i is the current with positive value for discharge and V denotes the output voltage (or terminal voltage) of the cell. V_o is the voltage drop on R_o and V_p is

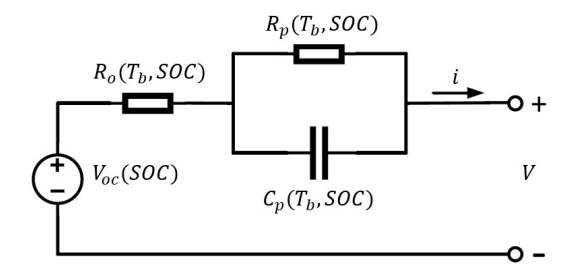


Fig. 4: The first-order equivalent circuit model

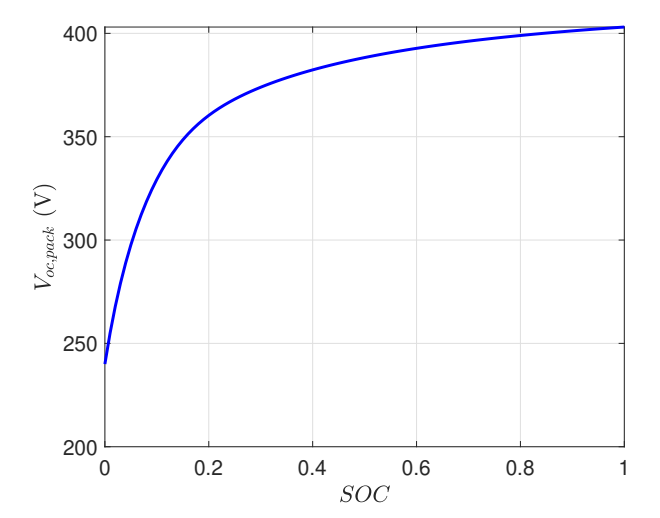


Fig. 5: Open circuit voltage values with respect to SOC.

the polarization voltage on R_p . The dynamics of the R-C pair can be represented by:

$$\dot{V}_p = -\frac{V_p}{R_p C_p} + \frac{i}{C_p},\tag{8}$$

and the terminal voltage of the battery is

$$V = V_{oc} - iR_o - V_p. (9)$$

In order to maintain the model's accuracy, it is crucial to take into account the variation of the open circuit voltage V_{oc} with respect to state-of-charge (SOC) [43]. Similarly, according to [16], variations of the ohmic resistance, polarization resistance and capacitance with respect to both battery temperature and SOC are also considered. The battery cell SOC dynamics is specified by Coulomb counting as follows.

$$S\dot{O}C_{cell,i} = -\frac{i}{3600 \times C_{cell}},$$
 (10)

where C_{cell} is the cell capacity in Ah.

We assume that the battery pack is grouped by identical cells with similar initial SOC in our simulations, with S cells in series and P cells in parallel. Since the dynamic response of the RC circuit has almost reached steady state after a brief period of time, it can be assumed that the current flowing

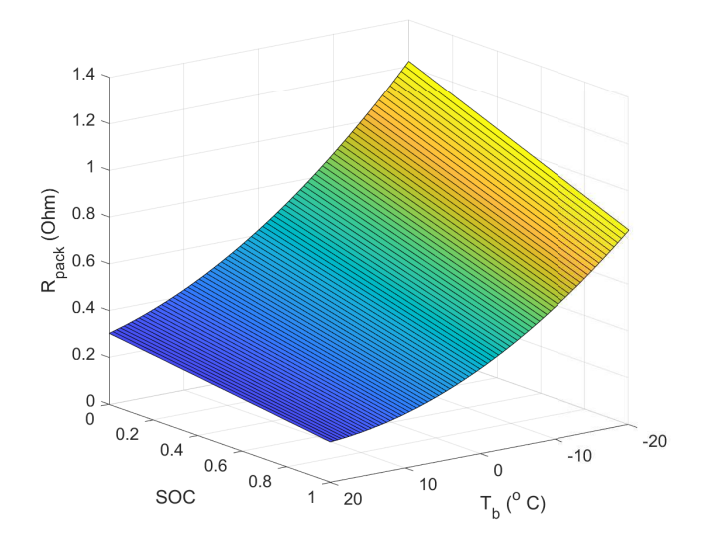


Fig. 6: Internal resistance of the battery pack with respect to SOC and battery temperature.

through the polarization resistor is equal to the overall current [35]. Hence one can write

$$R_{pack} = S(R_o + R_p), \tag{11a}$$

$$i_{pack} = Pi, (11b)$$

$$V_{oc,pack} = SV_{oc}, (11c)$$

where R_{pack} , i_{pack} and $V_{oc,pack}$ are the overall ohmic resistance of the battery pack, current of the battery pack and open circuit voltage of the battery pack, respectively. The internal resistance and the open circuit voltage of the battery pack used in our simulations correspond to the behaviors depicted in Figs. 5 and 6.

Furthermore, the battery pack SOC is the averaged SOC across the battery cells, which equals to, with the identical cell assumption, each battery cell's SOC. According to [1], [18], [36], the battery capacity is also dependent on the battery temperature, and we use the data from [1] to quantify the available percentage of battery capacity relative to the capacity at $25^{\circ}C$ versus battery temperature, as shown in Fig. 7.

For modeling the thermal behavior of the battery, the battery pack is considered as a lumped mass with specific heat capacity c_b , mass of m_b and temperature T_b . The battery is heated by the coolant which enters the battery from one side with high temperature T_1 (see Fig. 1), circulates around the battery and exits from the other side of the battery with cooled temperature T_2 . Therefore, one can write the differential equation for the battery temperature as:

$$C_b \dot{T}_b = R_{pack} i_{pack}^2 + \dot{m}_b c_c (T_1 - T_2) - h_a (T_a - T_b).$$
 (12)

Here $C_b = c_b m_b$ is the thermal inertia of the battery, and the first term on the right hand side considers the internal heat generation of the battery. The second term in (12) accounts for the heat from the coolant to the battery, and the third term is the heat transfer rate between battery and the ambient air, where T_a is the ambient air and h_a is the heat transfer

S, P	$c_{cb}[\frac{J}{kgK}]$	$c_c[\frac{J}{kgK}]$	$C_{pack}^{nom}[Ah]$	$m_{cb}[kg]$	$h_b[\frac{W}{m^2K}]$	$h_a[\frac{W}{K}]$	$m_{clnt}[kg]$
96, 3	840	2433	185	50	500	15	15
$m_b[kg]$	$c_b[\frac{J}{kgK}]$	η_{pump}	$\rho_c[\frac{kg}{m^3}]$	$m_{clnt,b}[kg]$	$m_{clnt,c}[kg]$	$G_{HX}[\frac{W}{K}]$	$c_a \frac{J}{kgK}$
250	1130	0.95	1114	11.75	3.25	400	1008
$\dot{m}_a[\frac{kg}{s}], m_a[kg]$	$m_{ca}[kg]$	$\dot{Q}_{met}[W]$	$\dot{Q}_{sol}[W]$	$\alpha_{cb}[\frac{W}{m^2K}]$	$\alpha_{ab}[\frac{W}{m^2K}]$	$\{A_b, A_{cb}\}[m^2]$	$A_{ab}[m^2]$
0.125, 0.129	4.25	400	200	30	500	${3,5}$	8

TABLE II: Parameters for the Proposed ITM Model.

TABLE III: Component modeling in the literature and their differences with our proposed model.

References	[19]	[20]	[22]	[24]	[25]	[27]	[29]	[30]	[32]	[33]	[34]	[35]	[41]	Ours
HP or AC loop		✓	✓	✓				✓					✓	✓
Battery	✓	✓	✓	✓	✓	✓	✓	✓	✓	✓		✓		✓
Pump		✓		✓	✓	✓					✓		✓	✓
Cabin air						✓	✓			✓	✓		✓	✓
Cabin HX							✓			✓	✓		✓	✓
Cabin body							✓			✓	✓		✓	✓
Traction power		✓	✓		√	✓			✓	✓		✓		✓
Liquid heating		✓				√			√		√	√		✓

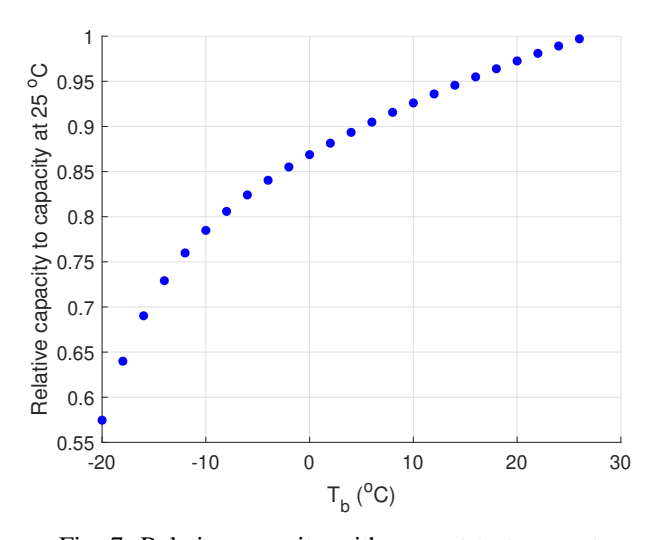


Fig. 7: Relative capacity with respect to temperature.

coefficient between the ambient air and the battery pack. Furthermore, according to the energy balance equation for the coolant, one can obtain the following thermal dynamic equation for coolant temperature:

$$C_2 \dot{T}_2 = \dot{m}_b c_c (T_1 - T_2) - h_b A_b (T_2 - T_b).$$
 (13)

In this equation, $C_2 = m_{clnt,b}c_c$ is the thermal inertia of the coolant mass that heats the battery and $m_{clnt,b}$ denotes the mass of the coolant around the battery. The first term on the right hand side characterizes the energy balance of the coolant and the second term accounts for the heat loss of the coolant when it transfers heat with the battery, where h_b is the heat transfer coefficient per unit area and A_b is size of the heat transfer surface area.

E. Battery power demand

The traction power demand for vehicle's movement can be written as [22]:

$$P_{trac} = V_{veh} \left(F_r + F_a + M \dot{V}_{veh} \right), \tag{14}$$

where V_{veh} , \dot{V}_{veh} , M, are vehicle speed, vehicle acceleration, and vehicle mass, respectively. The following formulas are used to compute the rolling (F_r) and aerodynamic (F_d) resistance forces:

$$F_r = C_r M g, (15a)$$

$$F_a = 0.5 \rho_a A_f C_d V_{veb}^2,$$
 (15b)

where C_r and C_d are, respectively, the rolling resistance and aerodynamic drag coefficients, A_f is the vehicle frontal area, and ρ_a is the air density. Combining the HP consumed power and electric pump power (6), the total thermal power required is

$$P_{TM} = P_{elec} + P_{pump}. (16)$$

Therefore, the total battery power can be denoted as

$$P_{tot} = P_{TM} + P_{trac}, (17)$$

and the battery pack current can be subsequently calculated by

$$i_{pack} = \frac{V_{oc,pack} - \sqrt{V_{oc,pack}^2 - 4R_{pack}P_{tot}}}{2R_{pack}}.$$
 (18)

Remark II.1. Maximizing the driving range of an EV is equivalent to maximizing the SOC at the end of its trip, which can be achieved by minimizing the current i_{pack} drawn from the battery at each time step and/or increasing the battery capacity by increasing battery temperature. According to (10), (17) and (18), battery current minimization can be achieved by

the following: 1) enabling battery charging from regenerative power by increasing battery temperature to charge-permitted value; 2) decreasing R_{pack} by increasing battery temperature to optimal value; and 3) decreasing P_{tot} by decreasing P_{TM} . Therefore, to maximize EV range for a short-term horizon, one can either increase battery temperature to optimal value, and/or decrease the thermal management power P_{TM} .

Table II lists all the parameters for the proposed ITM model. The differences between our proposed model for ITM of battery and cabin and other models found in related works for TM of battery and cabin are highlighted in Table III.

III. NONLINEAR MPC FORMULATION

In this section, we formulate the NMPC problem for the proposed ITM of battery and cabin heating, and investigate its cost function design and calibration. Recall that the governing equations of the ITM system are described in the previous section. Herein, we compactly denote the continuous-time nonlinear dynamics of the ITM system as follows

$$\dot{x} = f_c(x, u, p),\tag{19}$$

where the nonlinear continuous function $f_c(.)$ is the equations defined as (1)-(18), and the state vector x, control input vector u, and measured disturbance p are defined as follows

$$x = [SOC, T_b, T_3, T_1, T_2, T_6, T_{ca}, T_{cb}]^T, u = [\dot{m}_c, \dot{m}_b, n_{comp}]^T, \qquad p = P_{trac}.$$
 (20)

Consequently, the finite receding-horizon optimal control problem at each time step is defined as follows:

$$\min_{u} V(x_0, u) = \min_{u} \sum_{k=0}^{N-1} l(x(k), u(k)) + V_f(x(N))$$
 (21a)

s.t.
$$x(0) = x_0$$
, $x(k+1) = f_d(x(k), u(k))$ (21b)

$$x_{min} \le x(k) \le x_{max}, \ k = 0, \dots, N \tag{21c}$$

$$g_{min} \le g(u(k)) \le g_{max}, \ k = 0, \dots, N - 1.$$
 (21d)

In the above constrained optimal control problem (also denoted as $V_N^0(x_0)$), N is the prediction horizon, x_0 is the initial state, $f_d(.)$ is the discretized version of $f_c(.)$ with proper sampling time T_s , x_{min} and x_{max} are the lower and upper bound values of the states and g_{min} and g_{max} are the lower and upper bound values of the constraint function for control inputs. Specifically, the lower and upper bounds of the states in (21) are defined as:

$$x_{min} = [0, T_a, T_a, T_a, T_a, T_a, T_a, T_a]^T, x_{max} = [1, 35, 70, 70, 70, 70, 25, 25]^T,$$
(22)

where T_a presents the ambient temperature and all the temperatures are in Celsius degrees. The input constraints are defined by $g_{min} \leq g(u) = [u(1), u(2), u(3), u(1) + u(2)]^T \leq g_{max}$, where g_{min} and g_{max} are given by:

$$g_{min} = [0, 0, 0, 0]^T, \ g_{max} = [0.2, 0.2, 6000, 0.2]^T.$$
 (23)

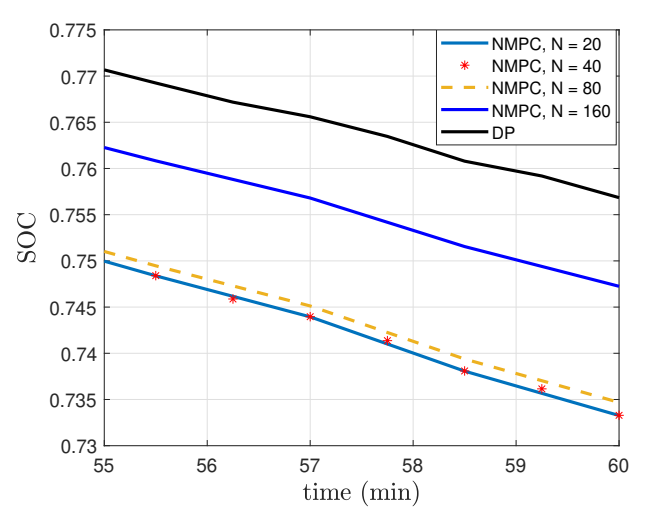


Fig. 8: Comparison of NMPC with cost function of (24a) and DP solution of (24).

A. NMPC stage cost selection

By regulating the temperatures of the passenger cabin and battery, the eventual goal is to simultaneously improve the EV range and satisfy the cabin heating requirements. For achieving this goal, the stage cost l(x(k),u(k)) of the defined NMPC problem (21) should be carefully selected. In this subsection, the DP technique, which provides a global optimal solution to an optimal control problem, is exploited to provide insights for designing the stage cost function. We first focus on the range maximization issue only, followed by the discussion on the cabin heating requirements in the next subsection.

We first apply DP to solve the following optimal control problem

$$\min_{N} -x_1(N) = -SOC(N) \tag{24a}$$

s.t.
$$(21b)$$
, $(21c)$, $(21d)$ $(24b)$

with $T_s = 4.5s$.

Remark III.1. The solutions to (24) obtained by DP will provide the global optimal state and control trajectories for the range maximization of the EV during the specified driving times. Compared to the optimal control problem (21) for NMPC, the horizon N for (24) is much longer and the cost function (24a) is highly nonlinear. Therefore, (24) is impractical for real-time control. Nevertheless, as shown below, the solution of (24) will provide very beneficial insights to design a cost function for NMPC that is suitable for real-time computation, while at the same time incurs minimum control performance loss as compared to (24).

To demonstrate that the cost function (24a) for DP cannot be directly used for NMPC (21), we simulate NMPC with cost function (24a) for various prediction horizon N, and compare their results to the DP. As plotted in the Fig. 8, it is clear that with a short prediction horizon that is suitable for real-time implementation, the positive impact of increasing battery temperature cannot be predicted, especially when the

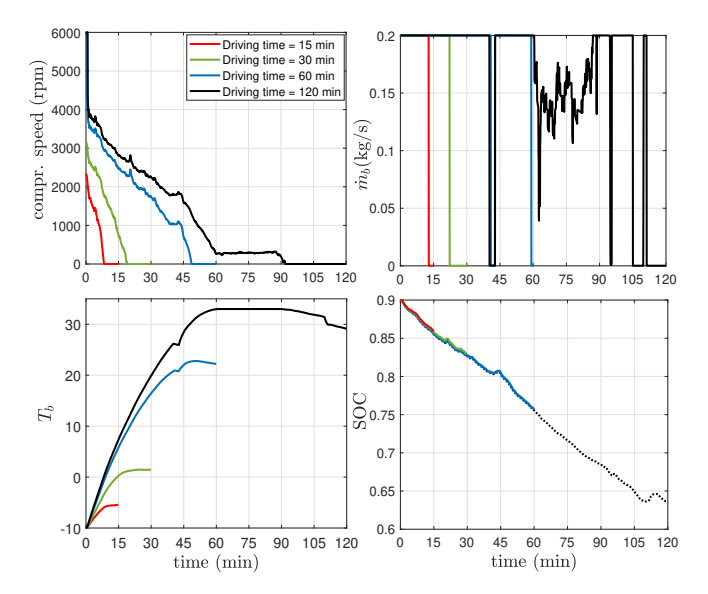


Fig. 9: DP solution of (24) for 4 different driving times, N = 200, 400, 800, 1600.

trip is long. In addition, even with a long prediction horizon of N=160, the advantages of battery heating in terms of range saving were only partially anticipated (in practice this long prediction horizon cannot be incorporated due to the cumbersome computational resources requirements). For other shorter horizons, the NMPC instead completely shuts off the battery heating to maximize the *short-term* battery SOC leading to a reduction of the EV range for medium to long-term driving times.

The optimization problem solved by DP will consider the maximization of range as the only objective function. To investigate the impact of driving time, four horizons are considered, namely, $N=200,\ 400,\ 800,\ 1600,\ corresponding to 15,30,60,120$ minutes of driving, respectively, representing short, medium, long and very long driving times. Furthermore, Fig. 9 shows the corresponding DP solution with an ambient temperature of $-10^{o}C$, based on which the following observations can be made:

- 1) According to Fig. 9, the optimal compressor speed and battery coolant flow rate, as determined by the DP solver, would result in heat being sent to the battery to increase battery temperature. Therefore, battery heating can contribute to EV range maximization. However, one can also observe from Fig. 9 that the optimal compressor speed is never at its maximum. This means the thermal management power (most of which is caused by the HP compressor) is not negligible so the optimal solution tries to strike a good trade-off between the energy consumption of the battery due to the thermal management system and the resulting energy saving of the battery due to the increased battery temperature.
- 2) According to Fig. 9, when the trip duration is longer, a more aggressive battery heating strategy is required. However, in practice, the trip information is usually not available beforehand. Therefore, we consider the worst case temperature and an average trip time to design the

stage cost l for all scenarios.

Based on these observations, we define the following stage cost l for (21) to balance the battery heating, the thermal management power consumption term, and the cabin comfort:

$$l(x,u) = P_{TM} + \alpha_1 (T_b - T_{b,sp})^2 + \alpha_2 (T_{ca} - T_{ca,sp})^2,$$
 (25)

where the first term penalizes the TM power, second term penalizes the deviation of battery temperature from its set point, and the last term penalizes the deviation of the cabin temperature from its set point; α_1,α_2 are the corresponding weights to express the trade-off between each terms. The set point temperature for cabin can be set by the passenger based on its own comfort, for current paper we choose $T_{ca,sp}=20^{o}C$ as a reasonable comforting temperature in a cold weather. For the battery, this temperature is also set to $T_{b,sp}=20^{o}C$ where the internal resistance is nearly at its minimum, according to Fig. 6. In addition, this temperature is a good operating temperature for battery considering its life time.

Remark III.2. We refer to the stage cost (25) as an indirect stage cost for simultaneously maximizing the EV range and satisfaction of the cabin heating requirements. In other words, to account for EV range maximization, the indirect approach uses battery temperature tracking plus the TM power penalization terms, while a direct approach will formulate the cost function similar to (24a) for the DP approach, since the latter directly relates to EV driving range and would lead to battery temperature optimization. See Remark II.1.

B. Stage cost weight tuning

Now that we have designed a stage cost function (25) for NMPC (21), let's focus on the weight-tuning of α_1 and α_2 to best address range improvement of the EV and to fulfill cabin heating requirements. As already mentioned in the previous section, different driving times can lead to different battery heating strategies, however, travel information is not usually accessible prior to the EV operation. In this regard, weight-tuning is carried out for a medium to long EV driving time in the worst case temperature (i.e., $-20^{\circ}C$). Note that in the simulation results presented in Section IV, we will show that this strategy works reasonably well for other driving times and conditions as well. We do the fine tuning of the weights in the following two steps.

a) Step 1: Let us define the following optimal control problem

$$\min_{u} \sum_{k=0}^{N-1} (T_{ca}(k) - T_{ca,sp})^{2} - \beta SOC(N)$$
 (26a)

s.t.
$$(21b)$$
, $(21c)$, $(21d)$, $(26b)$

which will then be solved by a DP solver. In other words, the optimal control problem (26) considers both the cabin heating requirement and the EV driving range in the cost function, with β being a tuning parameter to balance these two objectives. In this step, we optimize over β to find the best trade-off between the range and the cabin heating requirements. The results are shown in Fig. 10, where the final SOC relates to the EV driving

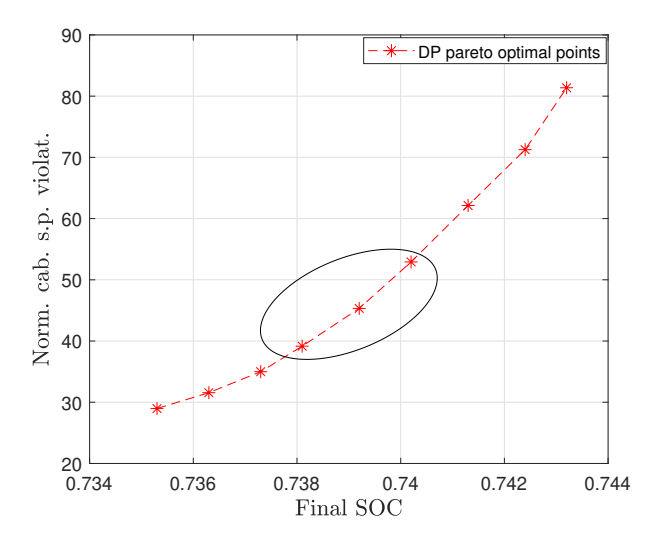


Fig. 10: Different trade-off between range and cabin set point violation by varying β in (26a). The points in the ellipse are used for weight tuning of NMPC shown in Fig. 11.

range and the cabin comfort is measured by the normalized cabin set point violation calculated by $\sum_{k=0}^{T_f} 10^{-3} (T_{ca,sp} - T_{ca}(k))^2$ with T_f being the final simulation time. Note that in Fig. 10, the points that are selected as reference points are marked with an ellipse and they represent an acceptable trade-off between the EV driving range and cabin comfort. The points on the left of the regions, although offer good satisfaction of the cabin heating requirements, suffer a lower EV range. The points on the right, however, give a better EV range but have worse cabin set point violations.

b) Step 2: Now that an acceptable trade-off has been identified using DP-based global solution, we will next find a good tuning for α_1 and α_2 in the NMPC cost function (25) such that the NMPC can achieve the similar trade-off as DP. This is done by a grid search over various combinations of α_1 and α_2 . The results are shown in Fig. 11, where the trade-offs between the range of EV and the normalized cabin set point violation by NMPC are shown with blue asterisks. Note that the reference DP points selected in Fig. 10 are also plotted in Fig. 11. Therefore, any weight combination within the marked region of Fig. 11 can achieve a similar optimal trade-off as DP, and hence provide an acceptable trade-off.

Remark III.3. The control goal, stage cost design, and weight-tuning procedure of our work is different with other related works concerning the thermal management of EVs for heating as follows. In [20] for the NMPC stage cost battery set point term and total thermal power terms are included but cabin heating requirement is neglected. In [35] the objective of the control is maximize the range, however again, cabin comfort requirements are not addressed. In [27] although the thermal management goal is to regulate the battery temperature for increasing its lifetime while satisfying cabin heating requirements, no discussion regarding the tradeoff between this two competing objective as well as optimality

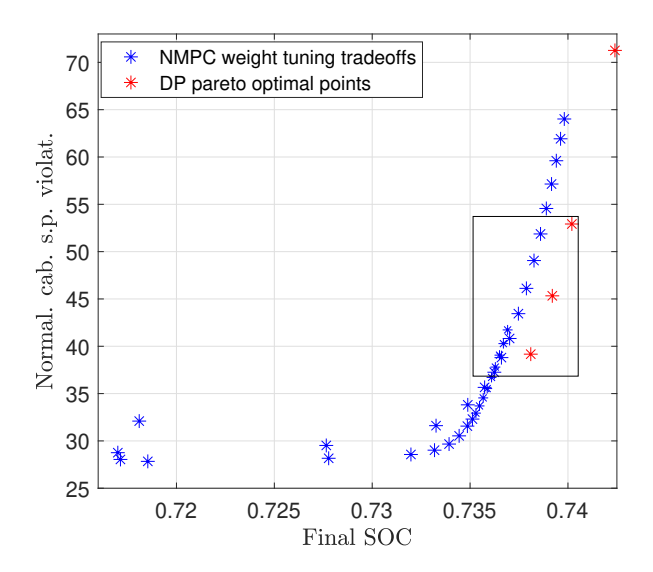


Fig. 11: Different trade-off between range and cabin set point violation by varying β in (26a) and α_1 and α_2 in the stage cost (25).

loss is done. In [34] the objective is to address the cabin comfort requirements in the cold weather conditions but battery thermal management is neglected.

C. Other considerations

When designing NMPC, another important consideration is the prediction horizon. While limited by the real-time computation capability, one may want to choose the longest prediction horizon that the microprocessor can handle. In addition to bringing the applied optimum control closer to the DP solution, a longer time horizon for NMPC offers an additional benefit. That is, provided that an accurate forecast of future speeds is known, future traction power demand can be determined as well, and hence allowing for the planning of most optimal strategies. However, uncertainty in the longterm velocity predictions also prevents the incorporation of the long horizons for NMPC. To this end, the prediction horizon is chosen in a way to meet the computational capabilities on one hand, and on the other hand, necessary weight-tuning of the stage cost terms is done, as discussed above, to compensate for the short-sightedness of the NMPC.

Another practical consideration that should be taken into account while applying the control input is battery safety and longevity. To this end, when the optimal control input is calculated at each time step, certain criteria have to be checked first to determine whether or not certain corrections are needed. A procedure for checking and correcting the control input, especially considering battery safety and longevity criteria, is shown in Procedure 1. Briefly speaking, firstly, as shown in Line 13-23 and Line 25-35, the Li-ion cell's terminal voltage must be checked to ensure it is within a particular temperature-dependent range during charge and discharge, denoted by the symbols $V_{cut,ch}$ and $V_{cut,disch}$, respectively. Secondly, as shown in Line 31-34 and Line 36-39, during the EV operation, charging the battery by the regenerative power is

forbidden below a specific battery temperature (usually 0° C) to prevent battery degradation and decrease plating. In this regard, if the battery voltage or the regenerative charging criterion impose limit on the power output of the battery, resulting in a compromise between addressing the thermal management power demand and the traction power demand, priority should be given to the traction power demand. As a result, a separate controller overrides the NMPC control strategy and prioritizes the traction power, and the remaining power is assigned to the TM system, as shown in Line 20-23. (In practice, the TM power consumption is mostly dominated by the compressor power, so the power allocation task in the Procedure 1 is shown for the compressor only without the pump).

Remark III.4. The reason for not using PID to control the proposed ITM or having it as a baseline is that our system is a MIMO system, making PID control design difficult. The system takes \dot{m}_b , \dot{m}_c , and compressor speed n_{comp} as inputs, and has battery temperature (T_b) and cabin temperature (T_{ca}) as outputs. Designing PID controllers for MIMO system is not trivial, especially considering the fact that each input has an effect on all the outputs and cannot be decoupled from other inputs. One possible way to design PID is to use two setpoint tracking controllers, where one determines the amount of heat rate to battery and the other determines the heat rate to cabin. In this way, each PID controller commands one control input to track one system output, and the two PID controllers can calculate their control command independently. However, after PID controllers issue their respective commands, which are the heat rates to battery and cabin, one needs to obtain the actuator commands (i.e., \dot{m}_b , \dot{m}_c , and n_{comp}) for the system to implement. This can only be done by either a rulebased "inverse thermal model", or by defining an optimization problem with decision variables being \dot{m}_b , \dot{m}_c , and n_{comp} and the objective function to minimize the difference between the PID-commanded and predicted heat rates. The PID design with rule-based inverse model and optimization thus will not have the benefits of a conventional PID design due to the optimization step involved. This results from the fact that in our MIMO control problem, each output cannot be associated exclusively with one input, and input and state constraints are also present in our problem. It is worth noting that designing several PID for MIMO systems is also challenging in the industrial setting. For example, similar MIMO thermal systems exist in industry applications (e.g. engine thermal management) and practitioners are moving towards MPC controllers instead of multiple PID controllers [46].

IV. SIMULATION RESULTS

In this section, the simulation results of the proposed ITM system for battery and cabin heating are presented. The traction power parameters in Equation 15 are adopted from [21]. It is worth noting that each step of NMPC computation and implementation takes about 0.09 second¹, well below the

Procedure 1: Nonlinear MPC implementation of the integrated thermal management of battery and cabin heating

```
heating
 1 for k = 1 : k_{final} do
          Current state as initial condition: x_0 = x(k)
          Traction power data for time steps k: k+N-1:
            P_{trac,N} = [P_{trac}(0), \dots, P_{trac}(N-1)]^T;
          Maximum traction power allowed in the horizon:
 4
            P_{trac,max} = \frac{V_{oc,pack}^{2}(x_{0}(1))}{4(R_{o,pack}(x_{0}(2),x_{0}(1)))} - P_{TM,max}
          for i = 1 : N \text{ do}
 5
               if P_{trac,N}(i) > P_{trac,max} then
 6
                  P_{trac,N}(i) = P_{trac,max};
 7
 8
               end
 9
          end
          Solve (21) and obtain the optimal input control:
10
            u^0(:,1) \leftarrow \text{NMPC}(x_0);
          Given (P_{trac}(0), u^0(x_0, 1), x_0), calculate the
11
            current based on: i_{pack} \leftarrow (18);
12
            V_{oc,pack}(x_0(1)) - i_{pack}R_{pack}(x_0(2), x_0(1));
          if \frac{V_{pack}}{S} < V_{cut,disch} then
13
               V_{pack} \leftarrow SV_{cut,disch};
i_{pack} \leftarrow \frac{V_{oc,pack} - V_{pack}}{R_{o,pack}(x_0(2),x_0(1))};
P_{tot,max} = V_{pack}i_{pack};
14
15
16
               p = \min(P_{tot,max}, P_{trac,N}(0));
17
18
               P_{remain} = P_{tot,max} - p;
               Using (2):
                 P_{elec} \leftarrow \min(P_{remain}, P_{elec}(u^0(3, 1), T_a);
               if P_{elec} \neq P_{elec}(u^0(3,1),T_a) then
                     Solve for n_{comp} such that:
21
                       P_{elec} = \frac{\dot{Q}_{HP}(n_{comp}, T_a)}{COP_{HP}(n_{comp}, T_a)}
                     u^0(3,1) \leftarrow n_{comp};
22
23
               end
          end
24
          if \frac{V_{pack}}{S} > V_{cut,ch} then
25
               if x_0(2) > 0 then
26
                    V_{pack} \leftarrow SV_{cut,ch};
i_{pack} \leftarrow \frac{V_{oc,pack} - V_{pack}}{R_{o,pack}(x_0(2),x_0(1))};
P_{tot,max} = V_{pack}i_{pack};
p = P_{tot,max} - P_{elec}(u^0(3,1),T_a);
27
28
29
30
31
                    V_{pack} \leftarrow V_{oc,pack}(x_0(1));

p = -P_{elec}(u^0(3,1), T_a);
32
33
34
          end
35
          if x_0(2) < 0 and p + P_{elec}(u^0(3,1), T_a) < 0
36
               p = -P_{elec}(u^0(3,1), T_a);
37
               V_{pack} \leftarrow V_{oc,pack}(x_0(1));
38
39
          x(k+1) = f_d(x_0, u^0(:, 1), p)
40
41 end
```

¹As measured in a standard PC with 2.6 GHZ CPU and 16 GB of RAM.

TABLE IV: NMPC simulation parameters

$\{\alpha_1,\alpha_2\}_{ITM}$	T_s [s]	\overline{N}				
{90, 180}	4.5	20				
$\{\alpha_1, \alpha_2\}_{cabin}$	$V_{cut,disch}$ [V]	$V_{cut,ch}$ [V]				
$\{0, 50\}$	2.5	4.25				

considered discretization time step, i.e., $T_s=4.5$ seconds, for the dynamics of the ITM system. It is also worth noting that this sampling time is reasonable to use due to slow dynamics of the TM system (e.g., see [21], [33]) although some fast-varying parameter such as vehicle's acceleration, velocity, and traction power are needed to calculate the states of TM system. More specifically, we take the average of the fast-varying parameters between each time step and use that value for the next time step control signal calculations. Comparing $T_s=4.5s$ with the cases with shorter time steps (e.g. $T_s=0.5s$) our results didn't show any difference; but longer time-steps will result in more efficient NMPC implementation due to fewer number of optimization variables.

Three different control strategies are implemented and compared. In the first strategy, NMPC (21) with stage cost (25) is applied with $\{\alpha_1, \alpha_2\}$ set to be $\{90, 180\}$ according to the weight-tuning discussion in the previous section. This control strategy is denoted as "NMPC-ITM" since the NMPC will simultaneously optimize both EV range and cabin comfort. In the second strategy, NMPC (21) with stage cost (25) is simulated with $\{\alpha_1, \alpha_2\}$ set to be $\{0, 50\}$. In other words, NMPC will fulfill the cabin heating requirement only, without heating the battery. This strategy is denoted as "NMPC-cabin". The third strategy is a rule-based strategy that follows a simple logic [22]. In this strategy, when the battery or cabin temperatures are below their set poins, the compressor is set to its maximum speed. Furthermore, the flow rates for battery and cabin branches are divided according to a pre-selected ratio, which is calibrated by trialand-error to deliver the best trade-off between the range and cabin heating requirements. When both battery temperature and cabin temperature are above their set points, the thermal management system is turned off. Such a rule-based control strategy is summarized below

$$u_{rb} = \begin{cases} [0.15, 0.05, 6000]^T & \text{if } T_b < T_{b,sp} \text{ and} \\ & T_{ca} < T_{ca,sp}; \\ [0, 0.05, 6000]^T & \text{if } T_b \ge T_{b,sp} \text{ and} \\ & T_{ca} < T_{ca,sp}; \\ [0.2, 0, 6000]^T & \text{if } T_b < T_{b,sp} \text{ and} \\ & T_{ca} \ge T_{ca,sp}; \\ [0, 0, 500]^T, & \text{else.} \end{cases}$$
(27)

Table IV lists all the parameters for the three control strategies, i.e., NMPC-ITM, NMPC-cabin, and rule-based. Please also note that we did not include the DP method solution for comparison as it is computationally cumbersome to carry out DP for our extensive simulations considering the number of

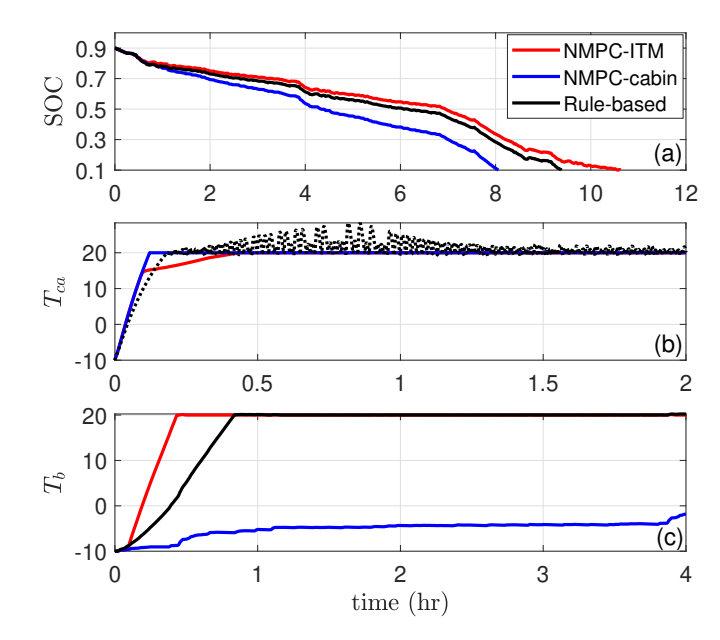


Fig. 12: SOC, cabin temperature and battery temperature vs time for a mixed driving cycle of HWFET and UDDS using 3 different control strategies. In comparison with the two other strategies, NMPC-ITM can extend the EV range while satisfying the cabin comfort requirements.

states of the system. In addition the main focus of this work is to compare the performances of the NMPC-based control strategies with a rule based strategy where all can be applied in practice, but DP cannot be applied in practice.

A. Comparisons for range and cabin comfort

In the first set of results, the three control strategies described above are compared with an ambient temperature of $T_a = -10^{\circ}C$. A mixed driving cycle of HWFET and UDDS is used for this simulation. The state initial condition vector is set to be $x_0 = [0.9, -10, -10, -10, -10, -10, -10, -10]^T$, i.e., the initial SOC is 90% and the initial temperatures are equilibrium with the ambient air. The simulation is terminated whenever the battery pack SOC drops below 0.1. The plot in Fig. 12(a) shows that the NMPC-ITM offers the best range with an increase of more than 2 hr driving time w.r.t the NMPC-cabin and more than 1 hr w.r.t the rule-based strategy. Additionally, since the weights are selected to provide optimal trade-off between driving range and cabin comfort, NMPC-ITM is able to address the cabin heating requirements by rapidly increasing the cabin temperature to around $15^{\circ}C$ in a short time and then smoothly converging to the set point temperature. See Fig. 12(b). The rule-based strategy also offers a better range w.r.t. the NMPC-cabin by increasing the battery temperature for higher efficiency. See Fig. 12(c). However, in this situation, the cabin temperature is fluctuating around the set point as a result of repetitive open/close switching of 3-way valve to adjust the cabin branch flow rate \dot{m}_c .

Next, we extend the simulation for two more ambient temperatures, i.e., $\{-20,0^{o}C\}$. Furthermore, to investigate the

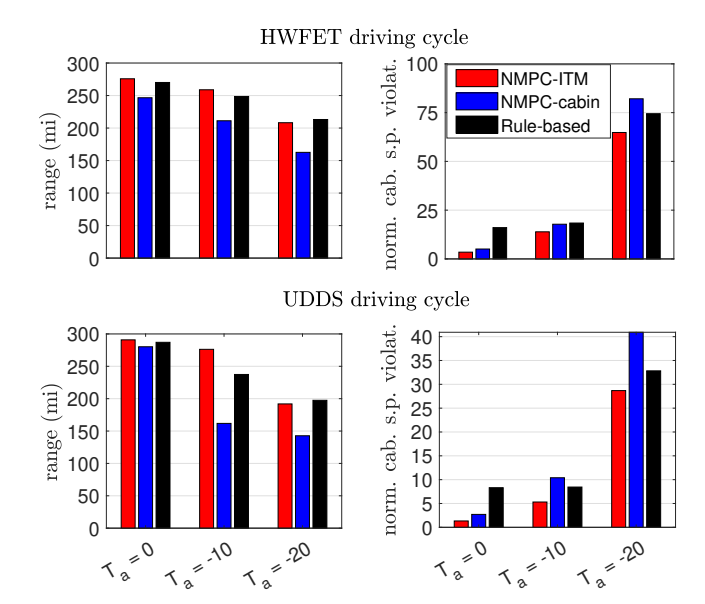


Fig. 13: Range and cabin set point violations under various impacting conditions. NMPC-ITM outperforms the other two strategies in various conditions considering these two metrics.

effect of driving cycle profile, HWFET and USDDS will be simulated separately (as opposed to being combined in Fig. 12). The results are plotted in Fig. 13, where the normalized cabin set point violation is calculated by $\sum_{k=0}^{T_f} \frac{1}{T_f} (T_{ca,sp} T_{ca}(k))^2$. By comparing the NMPC-ITM and NMPC-cabin together, it can be seen that the developed NMPC for ITM of battery and cabin heating has superior performance in all circumstances compared to the case when only cabin heating is performed. Noting that the accumulated cabin set point violation is normalized with the driving duration, the NMPCcabin has a higher normalized cabin set point violation than the NMPC-ITM, despite the fact that cabin temperature reaches its set point more quickly. It is also worth noting that for NMPCcabin, when the ambient temperature is -10 or $-20^{\circ}C$, the range of the EV for HWFET is greater than that of UDDS. The rationale is that in these extremely cold weather circumstances, driving intensity results in higher internal heat generation rate, which causes the battery temperature to increase more quickly and extends the EV range. For ambient temperatures 0 and $-10^{\circ}C$, better range and fulfillment of the cabin heating requirements are provided by the NMPC-ITM w.r.t the rule-based strategy. However, for an extremely cold weather condition, i.e., ambient temperature of $-20^{\circ}C$, a slight range advantage can be seen for the rule-based strategy, with a high price of sacrificing the cabin heating requirements.

B. Quantifying the benefits of NMPC-ITM in comparison with NMPC-cabin

The level of effectiveness of the proposed ITM system for heating (NMPC-ITM) is compared to the case where only cabin heating is allowed (NMPC-cabin). Recall that in Fig. 9 and its corresponding discussion, we noted that battery heating is necessary for any driving period in order to extend EV range. However, the degree of range increase still remains

unknown. In this regard, this investigation focuses on three critical factors in realizing the advantages of battery heating, i.e., driving time, driving behavior, and ambient temperature. To quantify the level of effectiveness of the NMPC-ITM against NMPC-cabin, we define $\Delta SOC(k) = SOC_{\text{ITM}}(k)$ – $SOC_{cabin}(k)$, where $SOC_{ITM}(k)$ is the SOC of the EV at time step k using the NMPC-ITM as the TM system and SOC_{cabin} is the same for NMPC-cabin. The variation of $\Delta SOC(k)$ w.r.t. several impact factors are shown in Fig. 14. For the ambient temperature of $0^{\circ}C$, since regenerative charging, as one of the most important factors in range extension, is enabled for both control strategies, the benefits of battery heating is not prominent compared to other ambient temperatures. However, when HWFET is used as the driving profile and when the trip is long, the SOC difference becomes significant, reaching to more than 3 \%. When the ambient temperature drops, the importance of the battery heating becomes more obvious. For example, for an ambient temperature of $-10^{\circ}C$ for both HWFET and UDDS driving cycle profiles, the benefits of battery heating are very significant for driving times more than 80 minutes.

Note that at the ambient temperature of $-10^{\circ}C$, the benefits of NMPC-ITM for shorter driving time is greater for the case of UDDS driving cycle than the HWFET cycle. This can be explained by Fig. 15. As can be seen, for both UDDS and HWFET driving cycles the battery temperature follows a similar trajectory using for NMPC-ITM. However, for NMPC-cabin, due to the higher intensity of the driving for HWFET profile and therefore higher internal heat generation, the battery temperature increases faster in the case of HWFET than the case of UDDS driving profile. As a result, regenerative charging is enabled sooner in HWFET and the internal resistance of the battery pack in each time step is also lower than in the UDDS case. Similar reasoning can be made for explaining the other cases with different ambient temperatures in Fig. 14 by considering the effect of internal resistance, regenerative charging and TM efficiency.

V. CONCLUSION

In this paper, we considered the problem of integrated battery and cabin heating for electric vehicles (EV) in cold conditions. An NMPC-based integrated thermal management (ITM) strategy for battery and cabin was developed to simultaneously optimize EV driving range and cabin comfort. Exhaustive modeling of different components of the ITM system were done. Since in NMPC a finite-horizon optimal control problem is solved at each time step where the optimal control trajectory is not necessarily the global optimal, a practical approach for the stage cost design and weight-tuning of the NMPC problem in comparison with the DP solution was developed to achieve driving range maximization while ensuring the cabin comfort. The developed NMPC-based ITM strategy was illustrated by comparing its performance to two additional benchmark strategies, i.e., rule-based control and cabin heating only. Numerical results showed the superiority of the proposed NMPC-based ITM strategy in comparison with the benchmarks. Finally, the impacts of several important factors, including the ambient temperature, driving cycle

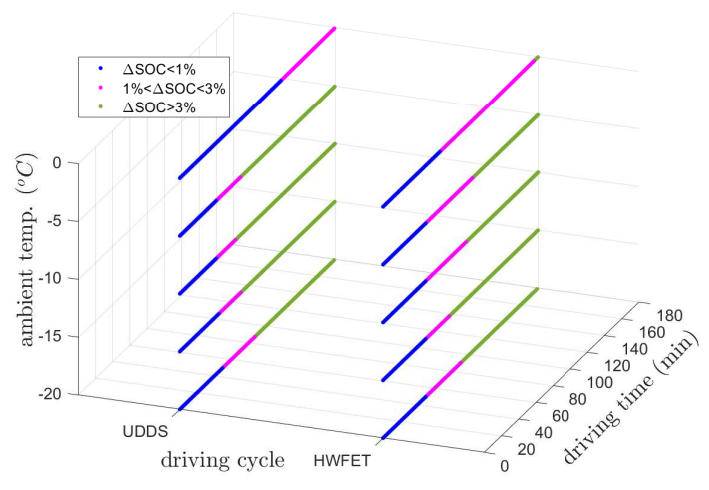


Fig. 14: Level of effectiveness of NMPC-ITM vs NMPC-cabin considering the most important factors for realizing the benefits of battery heating.

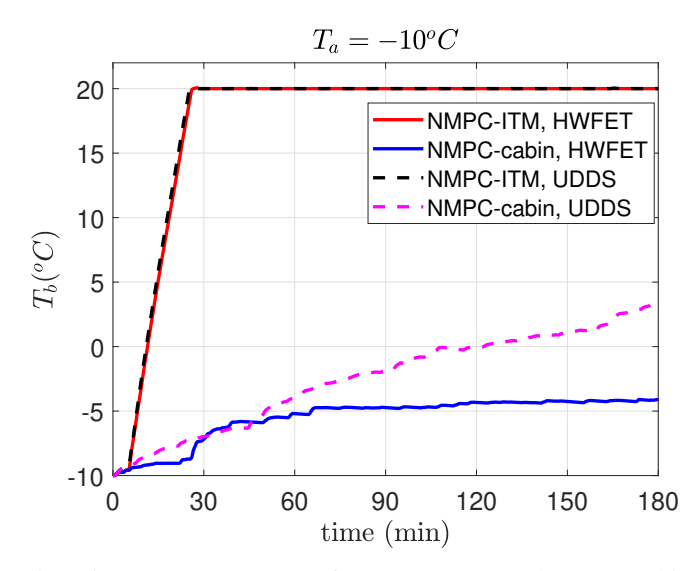


Fig. 15: Battery temperature for NMPC-ITM and NMPC-cabin under HWFET and UDDS driving profiles.

profile and behavior, and driving time, were also analyzed to summarize the operating conditions under which the proposed ITM is critically needed.

Future work will focus on improving the NMPC-based control strategies, e.g. by incorporating practical ways for having longer prediction horizons. Comparison with other benchmark control approaches will also be included in our future work.

REFERENCES

- A. A. Pesaran, S. Santhanagopalan, and G.-H. Kim, Addressing the impact of temperature extremes on large format li-lon batteries for vehicle applications. National Renewable Energy Laboratory, 2013.
- [2] S. Wu, R. Xiong, H. Li, V. Nian, and S. Ma, "The state of the art on preheating lithium-ion batteries in cold weather," *Journal of Energy Storage*, vol. 27, p. 101059, 2020.

- [3] W. D. Connor, Y. Wang, A. A. Malikopoulos, S. G. Advani, and A. K. Prasad, "Impact of connectivity on energy consumption and battery life for electric vehicles," *IEEE Transactions on Intelligent Vehicles*, vol. 6, no. 1, pp. 14–23, 2021.
- [4] S. Schoenberg, D. S. Buse, and F. Dressler, "Siting and sizing charging infrastructure for electric vehicles with coordinated recharging," *IEEE Transactions on Intelligent Vehicles*, vol. 8, no. 2, February 2023.
- [5] Z. Zhu, N. Pivaro, S. Gupta, A. Gupta, and M. Canova, "Safe model-based off-policy reinforcement learning for eco-driving in connected and automated hybrid electric vehicles," *IEEE Transactions on Intelligent Vehicles*, vol. 7, no. 2, pp. 387–398, 2022.
- [6] S. Xiao, X. Ge, Q.-L. Han, and Y. Zhang, "Resource-efficient platooning control of connected automated vehicles over vanets," *IEEE Transactions* on *Intelligent Vehicles*, vol. 7, no. 3, pp. 579–589, 2022.
- [7] J. Chen, M. Liang, and X. Ma, "Probabilistic analysis of electric vehicle energy consumption using MPC speed control and nonlinear battery model," in 2021 IEEE Green Technologies Conference, Denver, CO, April 7–9, 2021.
- [8] J. Chen, A. Behal, and C. Li, "Active cell balancing by model predictive control for real time range extension," in 2021 IEEE Conference on Decision and Control, Austin, TX, USA, December 13–15, 2021.
- [9] "California will ban sales of new gasoline-powered cars by 2035," https://www.npr.org/2022/08/25/1119456396/california-is-set-toban-sales-of-new-gasoline-powered-cars-by-2035, accessed: 2022-11-01.
- [10] S. Schaut, E. Arnold, and O. Sawodny, "Predictive thermal management for an electric vehicle powertrain," *IEEE Transactions on Intelligent* Vehicles, 2021.
- [11] Z. Zhou, C. Rother, and J. Chen, "Event-triggered model predictive control for autonomous vehicle path tracking: Validation using carla simulator," *IEEE Transactions on Intelligent Vehicles*, accepted for publication April 2022.
- [12] T. Mesbahi, N. Rizoug, P. Bartholomeüs, R. Sadoun, F. Khenfri, and P. Le Moigne, "Optimal energy management for a li-ion battery/supercapacitor hybrid energy storage system based on a particle swarm optimization incorporating nelder-mead simplex approach," *IEEE Transactions on Intelligent Vehicles*, vol. 2, no. 2, pp. 99–110, 2017.
- [13] F.-Y. Wang, "A new phase of IEEE Transactions on Intelligent Vehicles: Being smart, becoming active, and believing intelligent vehicles," *IEEE Transactions on Intelligent Vehicles*, vol. 8, no. 1, pp. 3–15, 2023.
- [14] C. Yang, R. Chen, W. Wang, Y. Li, X. Shen, and C. Xiang, "Cyber-physical optimization-based fuzzy control strategy for plug-in hybrid electric buses using iterative modified particle swarm optimization," *IEEE Transactions on Intelligent Vehicles*, 2023.
- [15] S. Teng, L. Chen, Y. Ai, Y. Zhou, Z. Xuanyuan, and X. Hu, "Hierarchical interpretable imitation learning for end-to-end autonomous driving," *IEEE Transactions on Intelligent Vehicles*, vol. 8, no. 1, pp. 673–683, 2023
- [16] J. Jaguemont, L. Boulon, and Y. Dubé, "Characterization and modeling of a hybrid-electric-vehicle lithium-ion battery pack at low temperatures," *IEEE Transactions on Vehicular Technology*, vol. 65, no. 1, pp. 1–14, 2015.
- [17] ——, "A comprehensive review of lithium-ion batteries used in hybrid and electric vehicles at cold temperatures," *Applied Energy*, vol. 164, pp. 99–114, 2016.
- [18] N. Shidore and T. Bohn, "Evaluation of cold temperature performance of the jcs-vl41m phev battery using battery hil," *Evaluation*, vol. 1, p. 1333, 2008.
- [19] Y. Ma, H. Ding, H. Mou, and J. Gao, "Battery thermal management strategy for electric vehicles based on nonlinear model predictive control," *Measurement*, vol. 186, p. 110115, 2021.
- [20] Y. Ma, H. Ding, Y. Liu, and J. Gao, "Battery thermal management of intelligent-connected electric vehicles at low temperature based on nmpc," *Energy*, vol. 244, p. 122571, 2022.
- [21] M. R. Amini, H. Wang, X. Gong, D. Liao-McPherson, I. Kolmanovsky, and J. Sun, "Cabin and battery thermal management of connected and automated hevs for improved energy efficiency using hierarchical model predictive control," *IEEE Transactions on Control Systems Technology*, vol. 28, no. 5, pp. 1711–1726, 2019.
- [22] M. R. Amini, I. Kolmanovsky, and J. Sun, "Hierarchical mpc for robust eco-cooling of connected and automated vehicles and its application to electric vehicle battery thermal management," *IEEE Transactions on Control Systems Technology*, vol. 29, no. 1, pp. 316–328, 2020.
- [23] J. Lopez-Sanz, C. Ocampo-Martinez, J. Alvarez-Florez, M. Moreno-Eguilaz, R. Ruiz-Mansilla, J. Kalmus, M. Gräeber, and G. Lux, "Nonlinear model predictive control for thermal management in plug-in hybrid

- electric vehicles," *IEEE Transactions on Vehicular Technology*, vol. 66, no. 5, pp. 3632–3644, 2016.
- [24] S. Park and C. Ahn, "Computationally efficient stochastic model predictive controller for battery thermal management of electric vehicle," *IEEE Transactions on Vehicular Technology*, vol. 69, no. 8, pp. 8407–8419, 2020
- [25] Y. Xie, C. Wang, X. Hu, X. Lin, Y. Zhang, and W. Li, "An mpc-based control strategy for electric vehicle battery cooling considering energy saving and battery lifespan," *IEEE Transactions on Vehicular Technology*, vol. 69, no. 12, pp. 14657–14673, 2020.
- [26] T. Fischer, T. Kraus, C. Kirches, and F. Gauterin, "Demonstration of a nonlinear model predictive control of a thermal management system for electric vehicles in real-time," in 2018 IEEE Conference on Control Technology and Applications (CCTA). IEEE, 2018, pp. 676–682.
- [27] H. Min, Z. Zhang, W. Sun, Z. Min, Y. Yu, and B. Wang, "A thermal management system control strategy for electric vehicles under lowtemperature driving conditions considering battery lifetime," *Applied Thermal Engineering*, vol. 181, p. 115944, 2020.
- [28] C. Zhu, F. Lu, H. Zhang, J. Sun, and C. C. Mi, "A real-time battery thermal management strategy for connected and automated hybrid electric vehicles (cahevs) based on iterative dynamic programming," *IEEE Transactions on Vehicular Technology*, vol. 67, no. 9, pp. 8077– 8084, 2018.
- [29] S. Zhao and C. C. Mi, "A two-stage real-time optimized ev battery cooling control based on hierarchical and iterative dynamic programming and mpc," *IEEE Transactions on Intelligent Transportation Systems*, 2021.
- [30] Y. Ma and J. Li, "Iterative dynamic programming strategy for electric vehicle battery thermal management optimization," *Advanced Theory and Simulations*, p. 2100602, 2022.
- [31] J. Cen and F. Jiang, "Li-ion power battery temperature control by a battery thermal management and vehicle cabin air conditioning integrated system," *Energy for Sustainable Development*, vol. 57, pp. 141–148, 2020.
- [32] Y. Masoudi, A. Mozaffari, and N. L. Azad, "Battery thermal management of electric vehicles: An optimal control approach," in *Dynamic Systems and Control Conference*, vol. 57243. American Society of Mechanical Engineers, 2015, p. V001T13A003.
- [33] Y. Liu and J. Zhang, "Electric vehicle battery thermal and cabin climate management based on model predictive control," *Journal of Mechanical Design*, vol. 143, no. 3, 2021.
- [34] J. Glos, L. Otava, and P. Václavek, "Non-linear model predictive control of cabin temperature and air quality in fully electric vehicles," *IEEE Transactions on Vehicular Technology*, vol. 70, no. 2, pp. 1216–1229, 2021.
- [35] S. Zhang and W. Shen, "Rule-based control of battery external heating for electric vehicle during driving at low temperatures," *IEEE Access*, vol. 9, pp. 149 360–149 371, 2021.
- [36] M. Sarmiento-Carnevali, A. Fly, and P. Piecha, "Electric vehicle cold start range estimation through battery-in-loop simulations within a virtual driving environment," 2020.
- [37] S. Mao, M. Han, X. Han, J. Shao, Y. Lu, L. Lu, and M. Ouyang, "Analysis and improvement measures of driving range attenuation of electric vehicles in winter," *World Electric Vehicle Journal*, vol. 12, no. 4, p. 239, 2021.
- [38] N. Mancini, J. S. M. Mardall, J. Kopitz, C. R. O'donnell, D. F. Hanks, and H. Li, "Optimal source electric vehicle heat pump with extreme temperature heating capability and efficient thermal preconditioning," Apr. 6 2021, uS Patent 10,967,702.
- [39] L. Feng and P. Hrnjak, "Experimental study of an air conditioningheat pump system for electric vehicles," SAE International Journal of Passenger Cars-Mechanical Systems, vol. 9, no. 1, pp. 68–74, 2016.
- [40] C. Liu, Y. Zhang, T. Gao, J. Shi, J. Chen, T. Wang, and L. Pan, "Performance evaluation of propane heat pump system for electric vehicle in cold climate," *International Journal of Refrigeration*, vol. 95, pp. 51–60, 2018.
- [41] I. Cvok, B. Škugor, and J. Deur, "Control trajectory optimisation and optimal control of an electric vehicle hvac system for favourable efficiency and thermal comfort," *Optimization and Engineering*, vol. 22, no. 1, pp. 83–102, 2021.
- [42] M. A. Fayazbakhsh and M. Bahrami, "Comprehensive modeling of vehicle air conditioning loads using heat balance method," SAE technical paper, vol. 2013, p. 1507, 2013.
- [43] X. Lin, H. E. Perez, S. Mohan, J. B. Siegel, A. G. Stefanopoulou, Y. Ding, and M. P. Castanier, "A lumped-parameter electro-thermal model for cylindrical batteries," *Journal of Power Sources*, vol. 257, pp. 1–11, 2014.

- [44] J. Chen, Z. Zhou, Z. Zhou, X. Wang, and B. Liaw, "Impact of battery cell imbalance on electric vehicle range," *Green Energy and Intelligent Transportation*, vol. 1, no. 3, pp. 1–8, December 2022.
- [45] T. Huria, M. Ceraolo, J. Gazzarri, and R. Jackey, "High fidelity electrical model with thermal dependence for characterization and simulation of high power lithium battery cells," in 2012 IEEE International Electric Vehicle Conference. IEEE, 2012, pp. 1–8.
- [46] M. Sun, Y. Hu, D. E. Edwards, J. Chen, I. Chang, and S. P. Moorman, "Active thermal management system and method for flow control," Apr. 26 2022, US Patent 11,312,208.



Mohammad R. Hajidavalloo received his B.Sc. and M.Sc. degree from University of Tehran in Mechanical Engineering in 2016 and 2018 respectively.

He is currently pursuing the Ph.D. degree in the department of Mechanical Engineering at Michigan State University. His research interests include Learning-Based Control, Model Predictive Control, and Optimal Control, with applications in Connected and Autonomous Vehicles.



Jun Chen (S'11-M'14-SM'20) received his Bachelor's degree in Automation from Zhejiang University, Hangzhou China, in 2009, and Ph.D. in Electrical Engineering from Iowa State University, Ames IA, USA, in 2014. Dr. Chen is currently an assistant professor at the ECE department at Oakland University. His research interests include artificial intelligence and optimal control, with applications in intelligent vehicles and energy systems.

Dr. Chen is a recipient of the NSF CAREER Award, the Best Paper Award from IEEE TRANSAC-

TIONS ON AUTOMATION SCIENCE AND ENGINEERING, the Faculty Recognition Award for Research from Oakland University, the Publication Achievement Award from Idaho National Laboratory, the Research Excellence Award from Iowa State University, and the Outstanding Student Award from Zhejiang University. He is/was an associate editor or editorial board member for IET Cyber-Systems and Robotics, Journal of Control and Decision, Energy Systems, IEEE International Conference on Robotics and Automation, IEEE Conference on Control Technology and Applications, and IFAC Symposium on Advances in Automotive Control. He is currently a Senior Member of the IEEE and a Member of SAE.



Qiuhao Hu received the B.S. and M.S. degrees in Naval Architecture and Ocean Engineering from Shanghai Jiao Tong University, Shanghai, China, and the Ph.D. degree in Naval Architecture and Marine Engineering from University of Michigan, Ann Arbor, MI, USA, in 2023. He is currently a research fellow with the Department of Naval Architecture and Marine Engineering, University of Michigan, Ann Arbor. His research interests are in hybrid electric systems, thermal and power management, battery management strategy, and optimal control.



Dr. Ziyou Song is an Assistant Professor with the Department of Mechanical Engineering at the National University of Singapore. He received B.E. degree (with honours) and Ph.D. degree (with highest honours) in Automotive Engineering from Tsinghua University, Beijing, China, in 2011 and 2016, respectively. After graduation, he worked as a Research Scientist at Tsinghua University from 2016-2017. From 2017 to 2019, he worked as a Postdoctoral Research Fellow at the University of Michigan, Ann Arbor, where he was also an Assistant Research

Scientist/Lecturer from 2019 to 2020. Prior to joining NUS, he was a Battery Algorithm Engineer at Apple Inc., Cupertino, US, where he was in charge of battery management system for Audio products (e.g., AirPods).

Dr Song's research interests lie in the areas of modelling, estimation, optimization, and control of energy storage (e.g., battery, supercapacitor, and flywheel) for electrified vehicles and renewable energy systems. Using energy storage as a bridge, his group is actively connecting the automotive, transportation, and power system communities by collaborating on interdisciplinary projects to ensure that both power system and transportation system are efficient, reliable, and clean. Dr. Song is the author or co-author of 2 book chapters and more than 60 peer-reviewed publications including 40 journal articles. He has received several paper awards, including Applied Energy 2015-2016 Highly Cited Paper Award, Applied Energy Award for Most Cited Energy Article from China, NSK Outstanding Paper Award of Mechanical Engineering, and 2013 IEEE VPPC Best Student Paper Award. Dr. Song serves as reviewer for more than 40 international journals. He also serves as Associate Editor for Automotive Innovation, SAE International Journal of Electrified Vehicles and IEEE Transactions on Transportation Electrification.



Xunyuan Yin received the Ph.D. degree in process control from the University of Alberta, Edmonton, AB, Canada, in 2018. He was a visiting student in the Department of Aerospace Engineering, the University of Michigan, Ann Arbor, MI, USA, in 2014.

He worked as a Postdoctoral Fellow at the University of Alberta. Currently, he is an Assistant Professor in the School of Chemistry, Chemical Engineering and Biotechnology at Nanyang Technological University, Singapore. He is a member

of the Early Career Advisory Board of IFAC Journal Control Engineering Practice. He was a recipient of the Izaak Walton Killam Memorial Scholarship, the Alberta Innovates Graduate Student Scholarship, the TW Fraser and Shirley Russell Teaching Fellowship, and Outstanding Reviewer for IEEE Transactions on Automatic Control and IEEE Transactions on Cybernetics. His research interests include process monitoring and control, learning-based process modeling, and their applications to complex industrial processes.



Dr. Zhaojian Li is an Assistant Professor in the Department of Mechanical Engineering at Michigan State University. He obtained M.S. (2013) and Ph.D. (2015) in Aerospace Engineering (flight dynamics and control) at the University of Michigan, Ann Arbor. As an undergraduate, Dr. Li studied at Nanjing University of Aeronautics and Astronautics, Department of Civil Aviation, in China. Dr. Li worked as an algorithm engineer at General Motors from January 2016 to July 2017. His research interests include Learning-based Control, Nonlinear and Complex

Systems, and Robotics and Automated Vehicles. He is the author of more than 40 top journal articles and several patents. He is currently the Associate Editor for Journal of Evolving Systems, American Control Conference and ASME Dynamics and Control Conference. He is a senior member of IEEE and a recipient of the NSF CAREER award.